Pd based bimetallic nanosheets for highly efficient nitrate reduction reaction

Yuanwei Ma[a,1], Jigang Wang[a,1], Qiang Liu[a], Zhongfang Li[a] and Likai Wang[a,b,c*]

[a] School of Chemistry and Chemical Engineering, Shandong University of Technology, Zibo, Shandong 255049, P. R. China

[b] School of Chemical and Biological Engineering, and Institute of Chemical Process, Seoul National University, Seoul 08826, Republic of Korea

[c] Key Laboratory of Advanced Energy Materials Chemistry (Ministry of Education), Nankai University, Tianjin 300071, China

* Corresponding author.

E-mail addresses: lkwangchem@sdut.edu.cn

[1]These authors contributed equally to this work.

Experimental section

Chemical regent

Palladium (II) acetylacetonate ($Pd(acac)_2$, 98%), Copper (II) acetylacetonate ($Cu(acac)_2$, 98%), Nickel (II) acetylacetonate ($Ni(acac)_2$, 98%), Iron (III) acetylacetonate ($Fe(acac)_3$, 99%), PVP (M=80000), oleylamine (OAm, $C_{18}H_{37}N$, 90%), molybdenum hexacarbonyl ($Mo(CO)_6$, 98%), glucose ($C_6H_{12}O_6 \cdot H_2O$), Sodium nitroprusside ($C_5H_4FeN_6Na_2O_3$), salicylic acid (AR, 99.5%), sodium hydroxide (NaOH, AR, 96%), trisodium citrate dihydrate (98%), potassium nitrate (KNO_3, 99%), ammonium chloride (NH_4Cl, ACS, 99.5%), potassium bicarbonate ($KHCO_3$, 99%), Zinc acetate ($Zn(Ac)_2$, AR, 99.0%), potassium nitrate-^{15}N ($K^{15}NO_3$, 98 atom%), Citric acid (99%), solution of sodium hypochlorite (NaClO, 0.1 M), methanol (CH_3OH, 99.7%), potassium hydroxide (KOH, 85%), The deionized (DI) water with a resistance of 18.25 MΩ·cm was obtained from the Milli-Q Plus System and used in the experiments.

Synthesis of PdNi nanosheet (PdNi NSs)

A solution was prepared by dissolving 24.2 mg of $Pd(acac)_2$, 16.1 mg of $Ni(acac)_2$, 30 mg of glucose, 15 mg of molybdenum hexacarbonyl and 12 mg of PVP in 5 mL of OAm with in a 50 mL glass vessel. The mixture was subjected to ultrasonic treatment for 60 min to ensure uniform dispersion of the surfactant in the oleylamine system. It was then rapidly heated to 220 ^oC in a heating mantle and stirred for 2 h. The resulting black products were collected and thoroughly washed three times with ethanol, followed by centrifugation at 10,000 rpm for 10 min. This process was repeated three more times using an ethanol-cyclohexane mixed solution under the same conditions, effectively removing the thin film deposited on the nanoparticles during synthesis. Finally, the black colloidal product was stored in cyclohexane for further use and labeled as PdNi NSs. Similarly, Pd, Ni, PdFeNi and PdCuFeNi were also prepared by the same procedure, with the only variable being the quantity of metal salts, while all other reaction conditions remained unchanged. The specific characteristics of each metal are detailed in Table S1.

Electrochemical measurements.

The electrochemical performance of the samples in the three-electrode system was evaluated using H-type cells separated by Nafion 115 membranes (DuPont). An electrochemical workstation (CHI 760E) with multiple channels was used to investigated the electrochemical data. In a typical three-electrode system, a carbon stick, an Ag/AgCl electrode, and the catalyst supported on carbon paper (loading: 200μg cm^{-2}) were used as the counter, reference, and working electrodes, respectively. The potential of the Ag/AgCl electrode was initially measured in both neutral and alkaline environments and subsequently converted to the reversible hydrogen electrode (RHE) scale using the equation: E (V vs. RHE) = E (vs. Ag/AgCl) + 0.197 V + 0.0591 × pH. For the electrocatalytic nitrate reduction, 0.1 M $KHCO_3$ and 0.05 M KNO_3 was used as the electrolyte, and 0.1 M KOH + 0.05 M KNO_3 was employed as the alkaline electrolyte. Then 35 mL of electrolyte were added into the anode and cathode compartments of the H-type cells, respectively. Chronoamperometry test was conducted at the stirring rate of 600 rpm for 0.5 h under -0.37 V, -0.47 V, -0.57 V, -0.67 V, -0.77 V and -0.87 V (vs. RHE), respectively. For the recycling stability test, the potentiostatic test was performed at -0.77 V with the stirring rate of 600 rpm for 0.5 h of each cycle. After each electrolysis cycle, the used electrolyte was removed and immediately replaced with fresh electrolyte, repeating the process 20 times. For the long-term chronoamperometry test, electrochemical measurements were performed at -0.77 V for an initial duration of 60,000 s. Upon completion of the reaction, the electrolyte was replaced with a fresh solution, and another 60,000 s electrolysis was conducted under identical conditions. Cyclic voltammetry (CV) curves were recorded in the non-Faradaic region at different scan rates to determine the electrochemical double-layer capacitance (C_{dl}). The electrochemically active surface area (ECSA) was then calculated using the equation: ECSA = C_{dl} / C_s, where C_s represents the specific capacitance (40 μF cm^{-2}). The solution resistance was tested at the potential of open circuit potential with frequencies ranging from 1000 kHz to 0.1 Hz.

Assembly of Zn-NO_3^- battery and the electrochemical measurements.

A typical H-type cell, separated by a bipolar membrane, was used to assemble the Zn-NO_3^- battery. The catalyst, supported on carbon paper, served as the cathode

(loading: 500μg cm^{-2}), while a polished Zn foil were employed as the anode. The cathode compartment contained 35 mL of electrolyte composed of 0.1 M $KHCO_3$ and 0.5 M KNO_3, whereas the anode compartment held 35 mL of electrolyte consisting of 6 M KOH and 0.2 M $Zn(Ac)_2$.

Isotope labeling experiments.

The isotope labeling experiments were conducted by using $Na^{15}NO_3$ as the feeding nitrogen source instead of $Na^{14}NO_3$. According to the aforementioned electrocatalytic method, 35 mL of electrolyte composed of 0.1 M $KHCO_3$ and 0.05 M $Na^{15}NO_3$ were added into the cathode compartment of H-type cell. After electrolysis for 1 h, the electrolyte was taken out and the pH was adjusted to weak acid (pH=2) by using 4 M H_2SO_4. Subsequently, 0.1 ml of maleic acid was introduced, resulting in the concentration of 400 ppm for maleic acid. 0.36 mL of above solution was mixed with 40 μL of deuterium oxide (D_2O) for the ^1H NMR test.

Product detection.

Determination of Ammonia.

The concentration of NH_3 was spectrophotometrically determined by using the indophenol blue method. First, the electrolyte was taken out from the electrochemical cell and diluted to the detection range. After that, 2 mL of solution was taken out and mixed with 2 mL of 1 M NaOH solution containing 5 wt.% salicylic acid and 5 wt.% trisodium citrate dihydrate. Then, 1 mL of 0.05 M NaClO solution and 0.2 mL of an aqueous solution of 1 wt.% $C_5H_4FeN_6Na_2O_3$ (sodium nitroferricyanide) were introduced. After the above mixture was kept in the dark at room temperature for 2 h. The absorption spectrum was determined using a UV-vis spectrophotometer (TU-1810APC) at the wavelength of 662 nm. The calibration curve of ammonia concentration and absorbance was prepared by using a series of standard ammonium chloride solutions.

Calculation of the Faradaic efficiency (FE) and yield rate (R).

In this work, the FE of NH_3 was calculated as follows:

$$FE_{NH_3} = \frac{8 * F * C_{NH_3} * V}{M_{NH_3} * Q} * 100\%$$

The yield rate (R) of NH_3 was calculated according to the following equation:

$$R_{NH_3} = \frac{C_{NH_3} * V}{M_{NH_3} * t * S} * 1000$$

where F is the Faraday constant (96485 C mol^{-1}), C_{NH3} represent the concentration of NH_3 (mg/L), V is the volume of the electrolyte (L), M_{NH3} denote the molar mass of NH_3 (mg/mol), Q is the total amount of charge (C), R is the yield rate (μmol h^{-1} cm^{-2}), t is the reaction time, S is the area of catalyst coated on the carbon cloth.

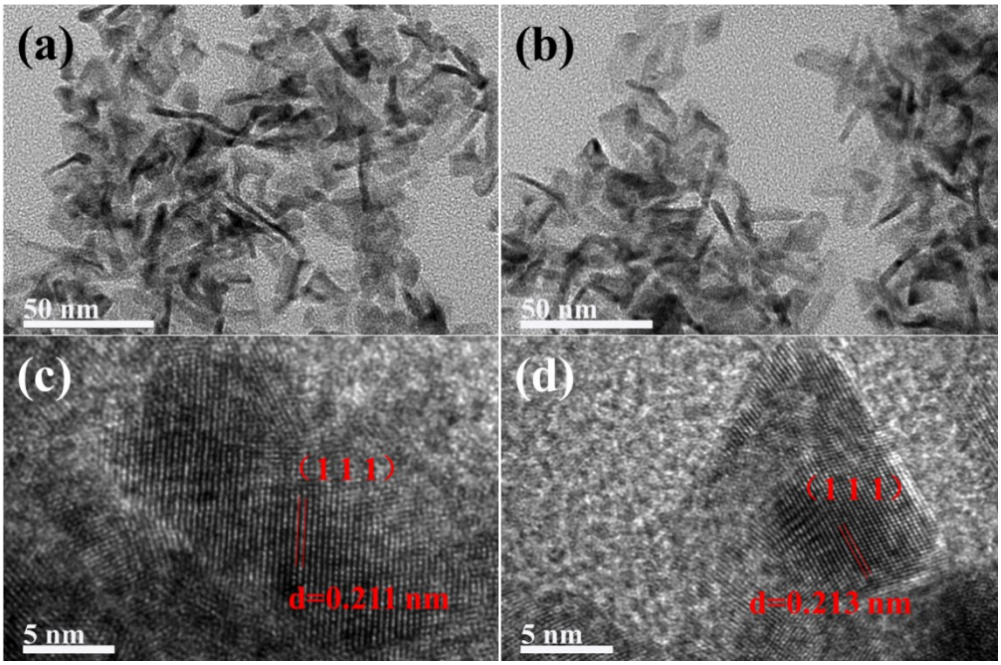

Fig. S1 Characterization of PdFeNi and PdCuFeNi. (a) and (b) TEM images,(c) and (d) HR-TEM images.

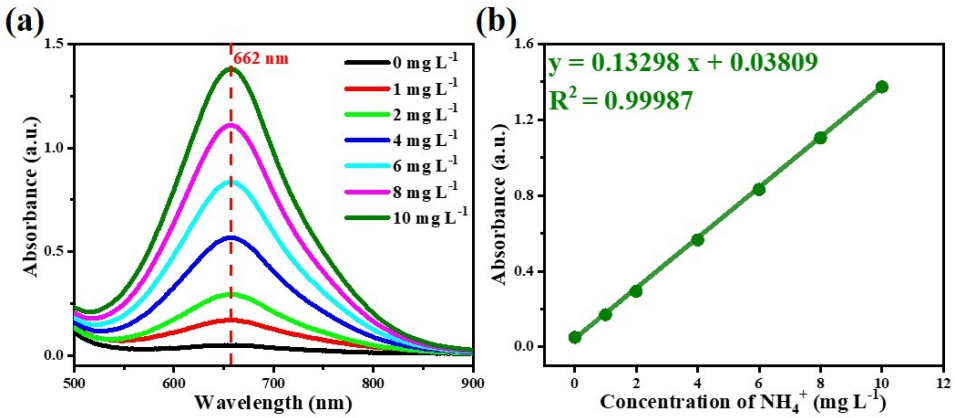

Fig. S2 The UV-vis calibration curve of NH_3 using different concentrations of NH_4Cl solutions as standards. UV-vis curves of assays with NH_4^+ ions (a) and linear fitting results of the calibration curves (b).

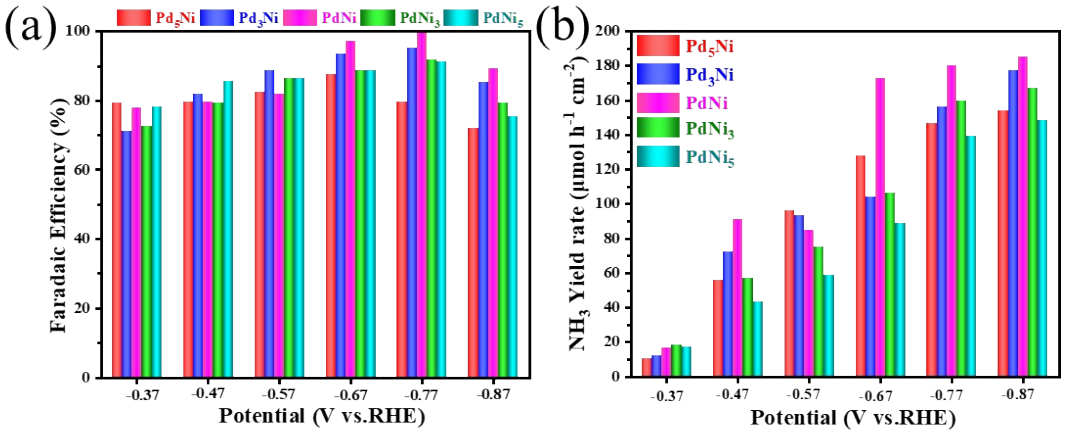

Fig. S3 (a) FE of NH_3, and (b) NH_3 yield rate of Pd_5Ni, Pd_3Ni, PdNi, $PdNi_3$ and $PdNi_5$ in 0.1 M $KHCO_3$ with 0.05 M KNO_3.

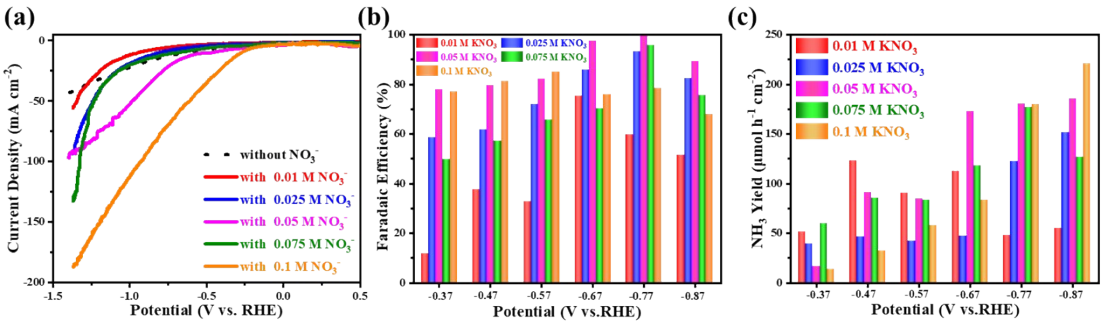

Fig. S4 Electrocatalytic nitrate reduction performance with different KNO_3 concentrations. (a) LSV curves of PdNi in 0.1 M $KHCO_3$ with or without KNO_3, (b) FE_{NH3}, and (c) NH_3 yield rate of PdNi NSs.

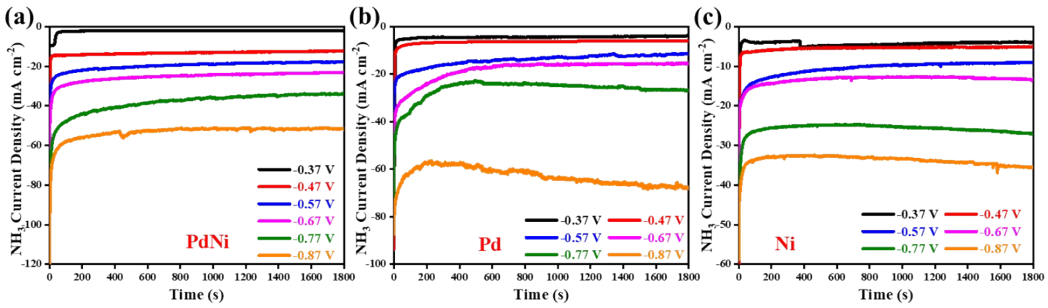

Fig. S5 The chronoamperometric curves of (a) PdNi NSs, (b) Pd, and (c) Ni at various potentials.

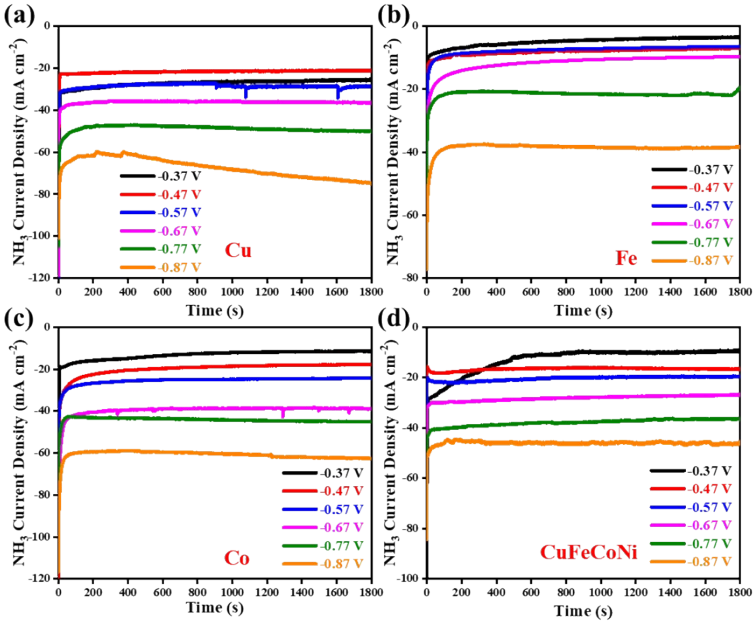

Fig. S6 The chronoamperometric curves of (a) Cu, (b) Fe, (c) Co and (d) CuFeCoNi at various potentials, respectively.

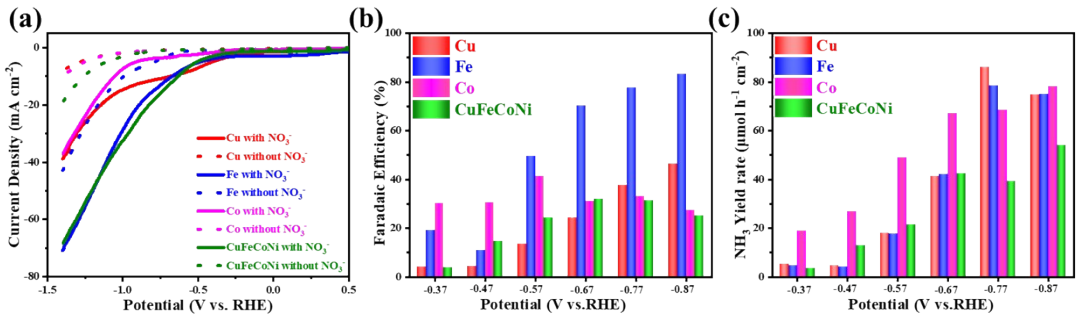

Fig. S7. Electrocatalytic nitrate reduction performance of Cu, Fe, Co and CuFeCoNi. (a) LSV curves of Cu, Fe, Co, and CuFeCoNi in 0.1 M $KHCO_3$ with or without 0.05 M KNO_3. NH_3 FE (b) and NH_3 yield rate (c) of Cu, Fe, Co and CuFeCoNi at various potentials.

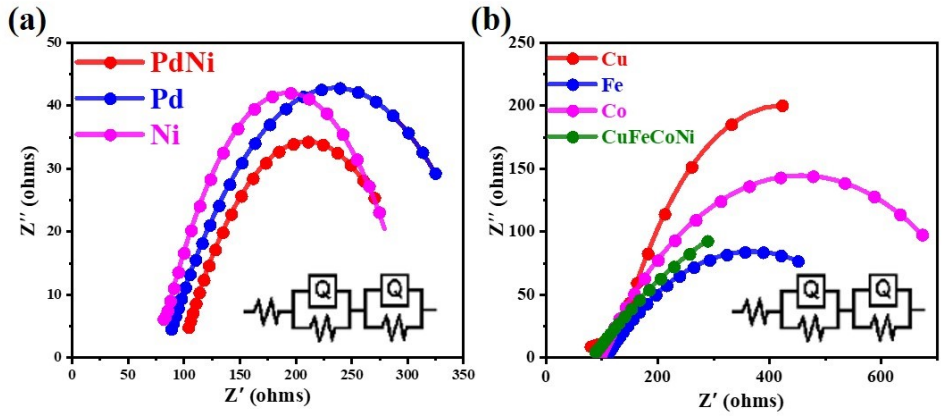

Fig. S8. Electrochemical impedance spectra in 0.1 M $KHCO_3$ + 0.05 M KNO_3. (a) The Electrochemical impedance spectra for PdNi NSs, Pd and Ni. (b) The Electrochemical impedance spectra for Cu, Fe, Co and CuFeCoNi.

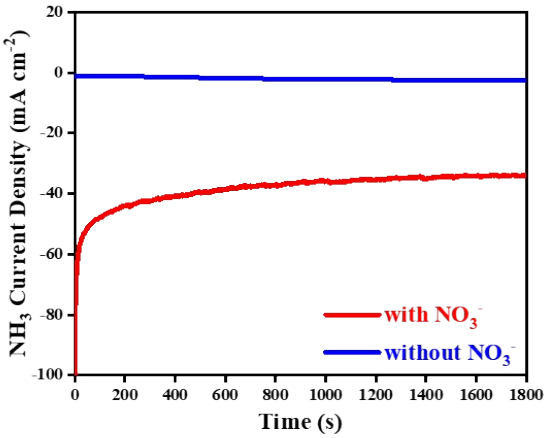

Fig. S9. The chronoamperometric curves of PdNi NSs with NO_3^- and without NO_3^- at -0.77 V.

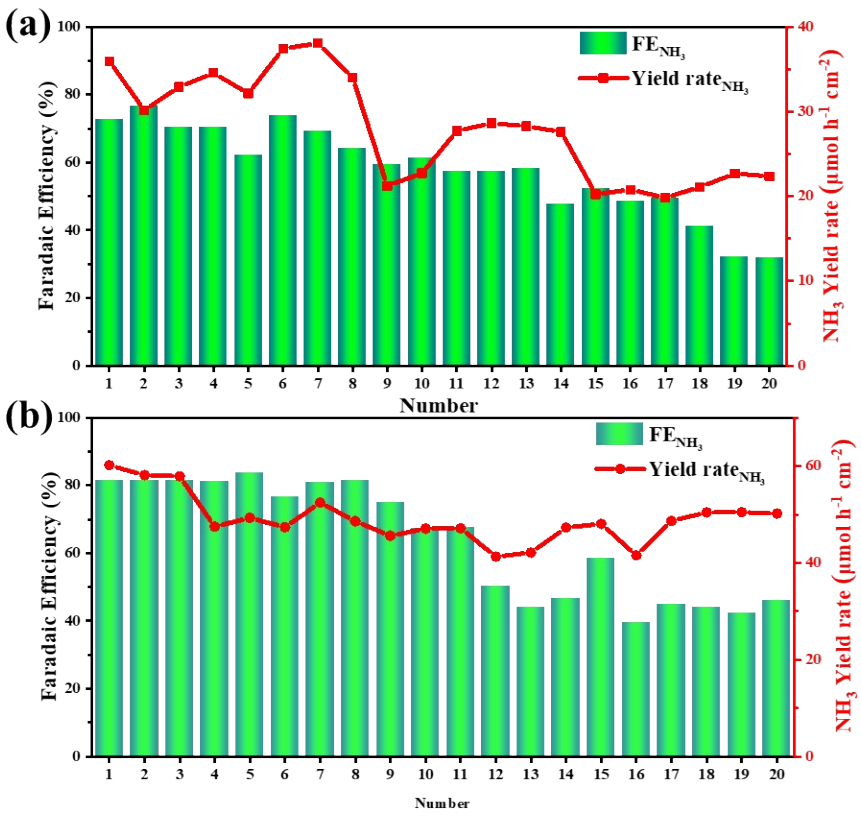

Fig. S10. The consecutive recycling electrolysis test of Pd (a)and Ni (b) at -0.77 V.

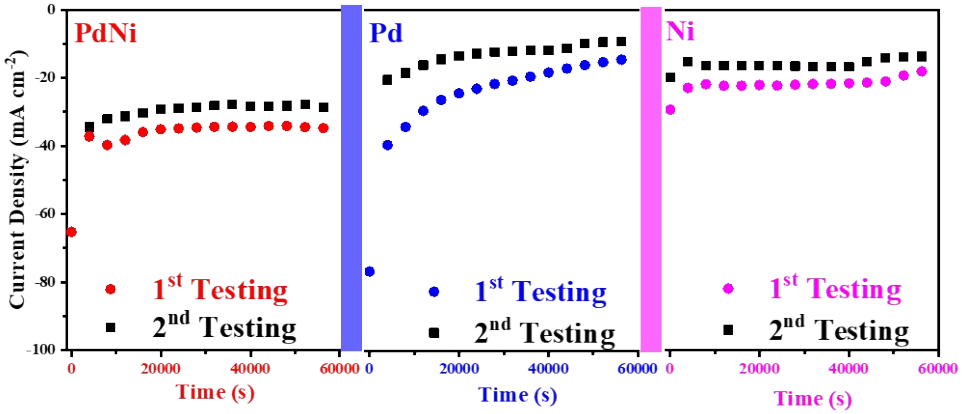

Fig. S11. Chronopotentiometry curves at -0.77 V of PdNi NSs, Pd, and Ni were tested for 60,000 s (1st Testing), and those of the electrolytes refreshed after 60,000 s (2nd Testing).

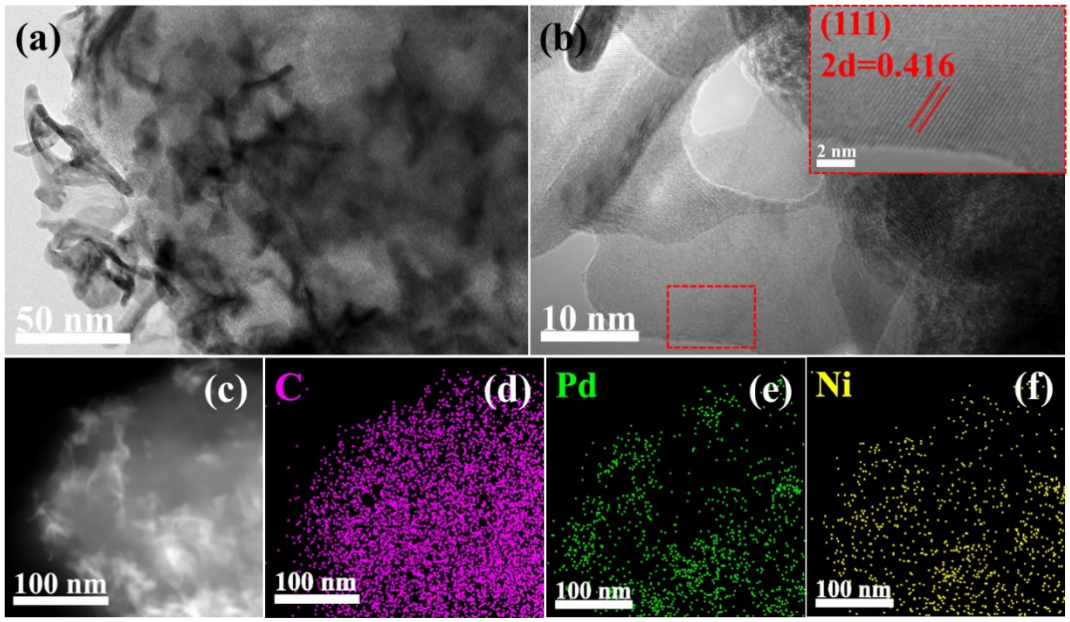

Fig. S12 TEM images of PdNi NSs catalyst after i-t curve stability test for 60,000 s at 0.1 M $KHCO_3$ and 0.05 M KNO_3. (a) TEM image of PdNi NSs. (b) HR-TEM image of PdNi NSs. HAADF-STEM images (c) and the corresponding EDS elemental mappings (d-f) of PdNi NSs.

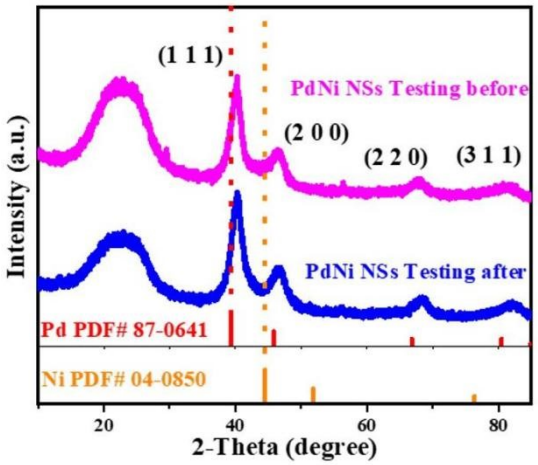

Fig. S13 XRD patterns of PdNi catalyst after i-t curve stability test for 60000 s at 0.1 M KOH.

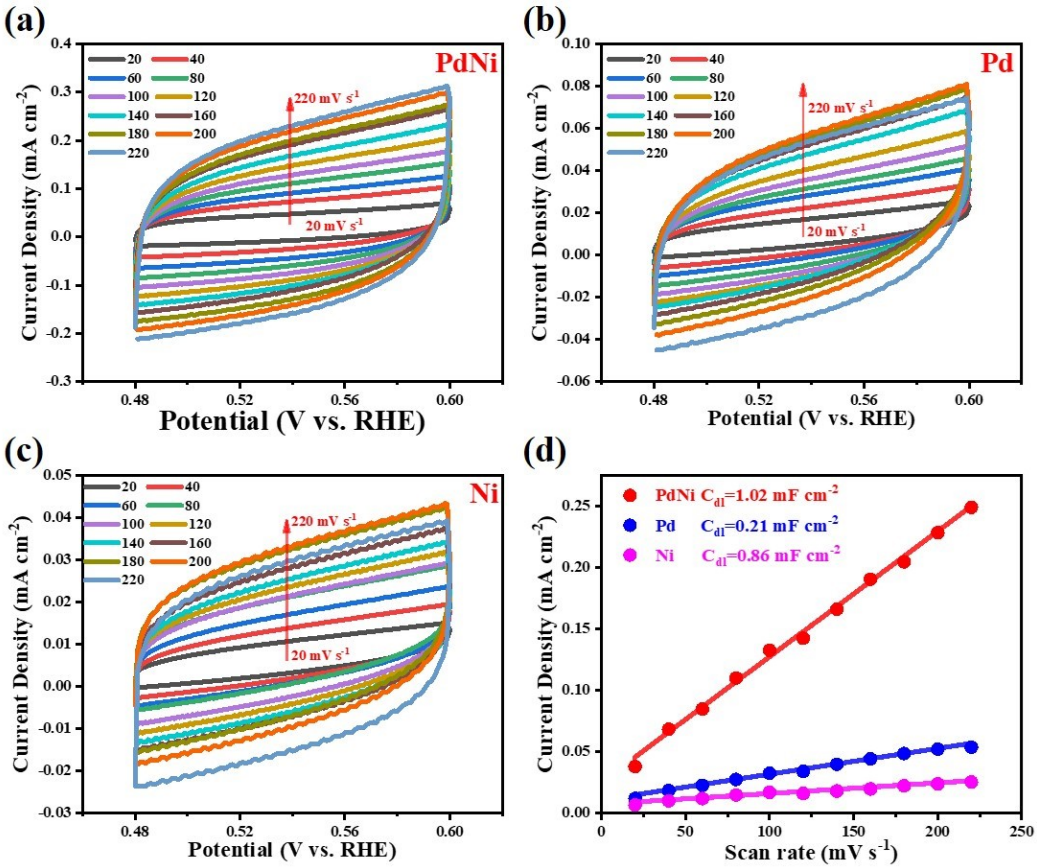

Fig. S14 Cyclic voltammetry (CV) profiles of (a) PdNi, (b) Pd and (c) Ni at sweep rates from 20 to 220 mV s^{-1}. (d) The correlation between current density and scan rate.

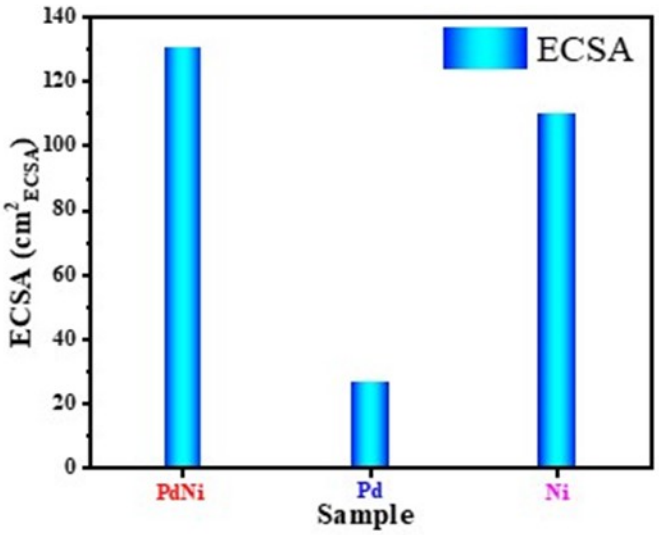

Fig. S15 The electrochemically active surface area (EASA) for PdNi NSs, Pd and Ni.

The ECSAs of the three samples were calculated as follow:

$$ECSA_{PdNi} = \frac{1.02\ mF\ cm^{-2}}{40\ \mu F\ cm^{-2}\ per\ 0.196\ cm^{-2}_{ECSA}} = 130.1\ cm^{2}_{ECSA}$$

$$ECSA_{Pd} = \frac{0.21\ mF\ cm^{-2}}{40\ \mu F\ cm^{-2}\ per\ 0.196\ cm^{-2}_{ECSA}} = 26.8\ cm^{2}_{ECSA}$$

$$ECSA_{Ni} = \frac{0.86\ mF\ cm^{-2}}{40\ \mu F\ cm^{-2}\ per\ 0.196\ cm^{-2}_{ECSA}} = 109.7\ cm^{2}_{ECSA}$$

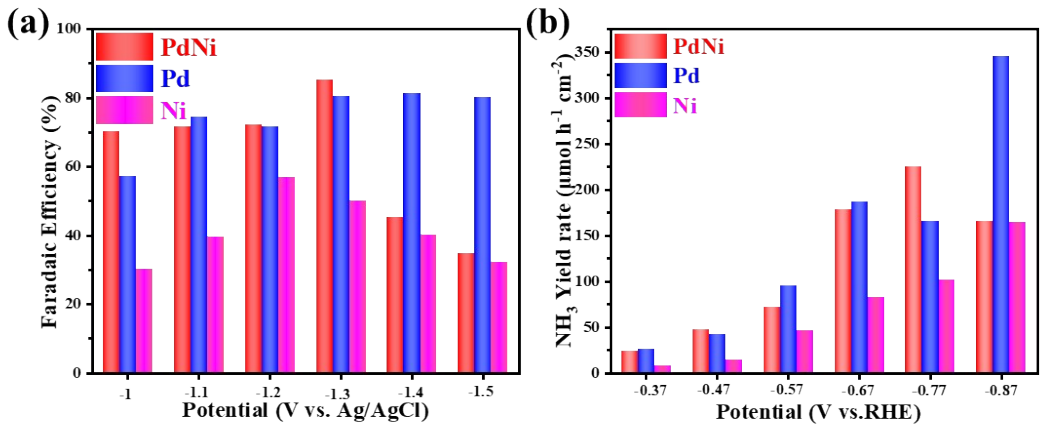

Fig. S16. Electrochemical NO_3RR performance in an alkali environment. (a) FE_{NH3} and (b) NH_3 yield rate of PdNi NSs, Pd and Ni in 0.1 M KOH with 0.05 M KNO_3.

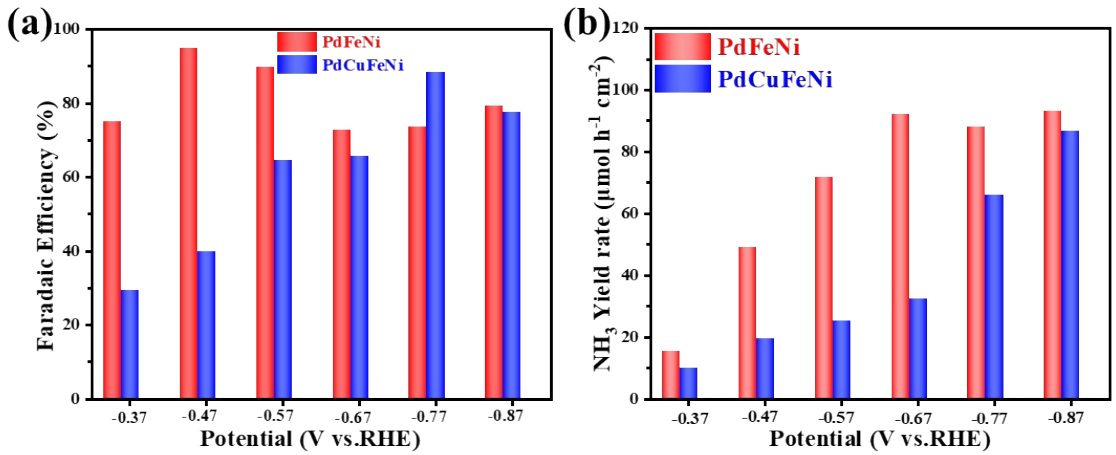

Fig. S17. Electrocatalytic nitrate reduction performance. (a) FE_{NH3} and (b) NH_3 yield rate of PdFeNi and PdCuFeNi at various potentials.

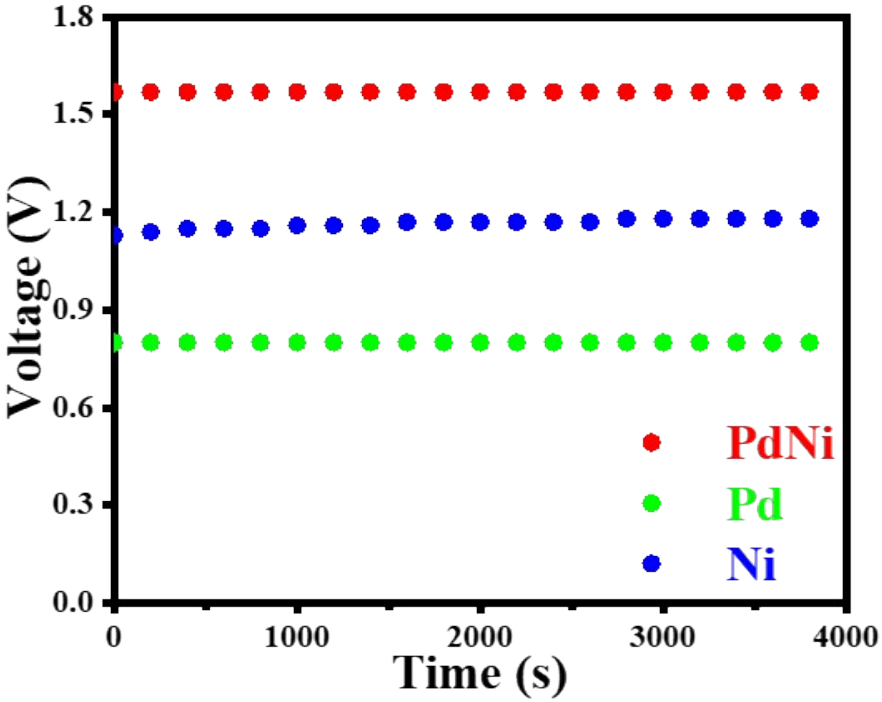

Fig. S18. OCP of Zn-NO_3^- battery in the rest period,

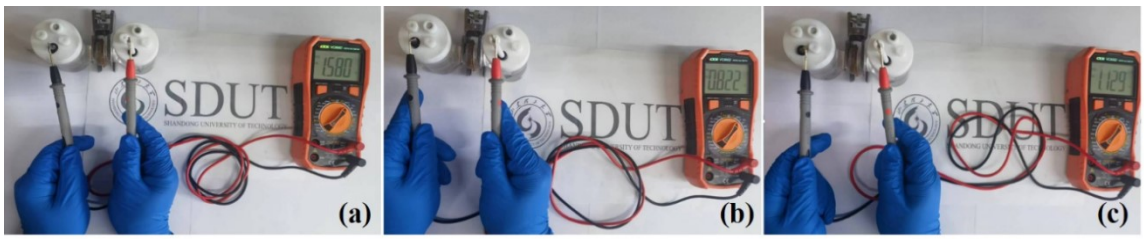

Fig. S19. (a) PdNi-based Zn-NO_3^- battery physical diagram of the open circuit voltage, (b) Pd-based Zn-NO_3^- battery physical diagram of the open circuit voltage, (c) Ni-based Zn-NO_3^- battery physical diagram of the open circuit voltage.

Table S1. Experimental details for as-prepared samples.

	samples		
	PdNi	**PdFeNi**	**PdCuFeNi**
$Pd(acac)_2$	24.2	16.8	13.6
$Cu(acac)_2$	——	——	9.1
$Fe(acac)_3$	——	11.2	9.1
$Co(acac)_2$	——	——	——
$Ni(acac)_2$	16.1	11.2	9.1

Table S2. Elemental content of Pd and Ni in PdNi NSs tested by ICP

	Wt %	At %
Pd	71.4	57.7
Ni	28.6	42.3

Table S3 Comparison of NH_3 yield and FE of different catalysts for NO_3RR.

Electrocatalyst	Electrolyte	NH_3 yield rates ($\mu mol\ h^{-1}\ cm^{-2}$)	FE_{NH3}	Potential (V vs. RHE)	Ref
PdNi	0.1 M $KHCO_3$ +0.05M KNO_3	181	99.6	-0.77	This Work
Fe-SnS_2/CC	0.5 M Na_2SO_4 +0.1M KNO_3	358	85.6	-0.7	[1]
FeOOH/CP	0.1 M PBS +0.1 M $NaNO_3$	58	94.3	-0.4	[2]
Cu-Fe_2O_3-60	0.5 M Na_2SO_4 +50 ppm KNO_3	108	88.47	-0.6	[3]
Fe-Co_3O_4	0.1 M PBS +50 mM KNO_3	38	95.5	-0.7	[4]
Pd/TiO_2	1 M LiCl +0.25 M $LiNO_3$	65	92.1	-0.7	[5]
Fe@N_{10}-C	500 ppm$NaNO_3$ +0.1 M Na_2SO_4	88	85.2	-0.75	[6]
O-Cu-PTCDa	0.1 M PBS +500 ppm KNO_3	25	85.9	-0.4	[7]
$NiFe_2O_4$/CC	0.1 M PBS + 0.1 M $NaNO_3$	175	96.6	-0.6	[8]
Fe/Ni_2P	0.2 M K_2SO_4 + 50 mM KNO_3	70	92.23	-0.75	[9]
TiO_2-NTs/CuO_x	0.5 M Na_2SO_4 + +100 ppm KNO_3	75	75	-0.5	[10]
RuFe NFs	0.5 M Na_2SO_4 0.1 M $NaNO_3$	15	92.9	-0.30	[11]
Co CNP	0.02 M Na_2SO_4 +100 ppm NO_3^-	17	92.0	-0.69	[12]
FOSP-Cu-0.1	0.5 M Na_2SO_4 +0.1 M KNO_3	101	93.91	-0.266	[13]
pCuO-10	0.05 M KNO_3 +0.05 M H_2SO_4	334	45	-0.7	[14]
CuFe-450	0.1 M PBS +3 mM NO_3^-	78	76.1	-0.8	[15]

BCDs/$NiCo_2O_4$/CC	0.5 M K_2SO_4 +200 ppm NO_3^-	174	100	-0.55	[16]
Cu/Cu_2O NWAs	0.5 M Na_2SO_4 +200 ppm NO_3^-	244	95.8	-0.85	[17]
a-RuO_2	0.5 M Na_2SO_4 +200 ppm NO_3^-	115	97.46	-0.35	[18]
NiPr-TPA-COF	0.5 M K_2SO_4 +0.1 M KNO_3	64	90	-1.38 (vs SCE)	[19]
Rh@Cu-0.6%	0.1 M Na_2SO_4 +0.1 M KNO_3	764	93	-0.2	[20]
$Pt_{0.9}/Ce_{0.5}$-SS	0.5 M Na_2SO_4 +0.1 M KNO_3	305	94.12	-0.5	[21]
Cu_2O/NF	0.5 M Na_2SO_4 +0.05 M NO_3^-	740	98.28	-0.8	[22]
Pd(111)	0.1 M Na_2SO_4 + 0.1 M NO_3^-	548.5	79.91	-0.7	[23]
Fe SAC	0.25 M K_2SO_4 +0.5 M NO_3^-	460	75	-0.66	[24]
PdCu/Cu_2O	0.5 M Na_2SO_4 +100 ppm NO_3^-	190	94.32	-0.8	[25]
PdW	0.5 M Na_2SO_4 + 0.1 M NO_3^-	135	70.8	-0.7	[26]
BC_2N/Pd	0.5 M Na_2SO_4 + 0.25 M NO_3^-	100	97.42	-0.3	[27]
Cu@C	1 mM NO_3^-	27.6	72	-0.3	[28]

Table S4. Comparison of OCP and power density of different catalysts for Zn-NO_3^- battery.

Electrocatalyst	PD (mW cm^{-2})	OCP (V vs. Zn)	Ref.
PdNi	11.3	1.56	This Work
Fe@C-900	12	1.3	29
Fe/Ni_2P	3.25	1.22	9
Pd/TiO_2	0.87	0.81	5
Fe-MoS_2	3.56	1.16	30
i-Ag/Co_3O_4 NWs	2.56	1.32	31
Co-TPA-E	8.46	1.32	32
Cu TABQ	12.3	0.8	33
Cu-RD	14.1	0.943	34
$NiCo_2O_4$	3.94	1.3	35
$ZnCo_2O_4$	4.62	1.52	36
CeO_{2-x}@NC/GP	3.44	1.45	37
fcc RuMo NFs	9.19	1.362	38
RhNi@Rh BMLs	10.5	1.394	39
W-O-CoP	9.27	0.7	40
NiRu ball-flower	10.0	1.39	41
MP-Cu	7.56	1.27	42

References

1. Chen, K.; Luo, Y.; Shen, P.; Liu, X.; Li, X.; Li, X.; Chu, K., Boosted nitrate electroreduction to ammonia on Fe-doped SnS_2 nanosheet arrays rich in S-vacancies. *Dalton Transactions* **2022,** *51* (27), 10343-10350.

2. Liu, Q.; Liu, Q.; Xie, L.; Ji, Y.; Li, T.; Zhang, B.; Li, N.; Tang, B.; Liu, Y.; Gao, S.; Luo, Y.; Yu, L.; Kong, Q.; Sun, X., High-Performance Electrochemical Nitrate Reduction to Ammonia under Ambient Conditions Using a FeOOH Nanorod Catalyst. *ACS Applied Materials & Interfaces* **2022,** *14* (15), 17312-17318.

3. Gao, Y.; Huang, K.; Yan, C.; Li, S.; Zhang, H.; Cheng, L.; Huang, F., Interfacial engineering of Cu-Fe_2O_3 nanotube arrays with built-in electric field and oxygen vacancies for boosting the electrocatalytic reduction of nitrates. *Materials Advances* **2022,** *3* (18), 7107-7115.

4. Wei, P.; Liang, J.; Liu, Q.; Xie, L.; Tong, X.; Ren, Y.; Li, T.; Luo, Y.; Li, N.; Tang, B.; Asiri, A. M.; Hamdy, M. S.; Kong, Q.; Wang, Z.; Sun, X., Iron-doped cobalt oxide nanoarray for efficient electrocatalytic nitrate-to-ammonia conversion. *Journal of Colloid and Interface Science* **2022,** *615*, 636-642.

5. Guo, Y.; Zhang, R.; Zhang, S.; Zhao, Y.; Yang, Q.; Huang, Z.; Dong, B.; Zhi, C., Pd doping-weakened intermediate adsorption to promote electrocatalytic nitrate reduction on TiO_2 nanoarrays for ammonia production and energy supply with zinc-nitrate batteries. *Energy & Environmental Science* **2021,** *14* (7), 3938-3944.

6. Shuo Zhang; Miao Lia; Jiacheng Li; Qinan Song; Liu, X., N-doped carbon-iron heterointerfaces for boosted electrocatalytic active and selective ammonia production. *Proceedings of the National Academy of Sciences* **2023**, e2207080119.

7. Chen, G.-F.; Yuan, Y.; Jiang, H.; Ren, S.-Y.; Ding, L.-X.; Ma, L.; Wu, T.; Lu, J.; Wang, H., Electrochemical reduction of nitrate to ammonia via direct eight-electron transfer using a copper-molecular solid catalyst. *Nature Energy* **2020,** *5* (8), 605-613.

8. Xie, L.; Hu, L.; Liu, Q.; Sun, S.; Zhang, L.; Zhao, D.; Liu, Q.; Chen, J.; Li, J.; Ouyang, L.; Alshehri, A. A.; Kong, Q.; Sun, X., High-performance electrochemical nitrate reduction to ammonia under ambient conditions using $NiFe_2O_4$ nanosheet arrays. *Inorganic Chemistry Frontiers* **2022,** *9* (14), 3392-3397.

9. Zhang, R.; Guo, Y.; Zhang, S.; Chen, D.; Zhao, Y.; Huang, Z.; Ma, L.; Li, P.; Yang, Q.; Liang, G.; Zhi, C., Efficient Ammonia Electrosynthesis and Energy Conversion through a Zn‐Nitrate Battery by Iron Doping Engineered Nickel Phosphide Catalyst. *Advanced Energy Materials* **2022,** *12* (13), 2103872.

10. Qiu, W.; Chen, X.; Liu, Y.; Xiao, D.; Wang, P.; Li, R.; Liu, K.; Jin, Z.; Li, P., Confining intermediates within a catalytic nanoreactor facilitates nitrate-to-ammonia electrosynthesis. *Applied Catalysis B: Environmental* **2022,** *315*, 121548.

11. Yunhao Wanga; Mingzi Sun; Jingwen Zhou; Yuecheng Xiong; Qinghua Zhang; Chenliang Yee; Xixi Wanga; Pengyi Lu; Tianyi Feng; Fengkun Hao; Fu Liu; Juan Wang; Yangbo Ma; Jinwen Yin; Shengqi Chu; Lin Gu; Bolong Huang; Fan, Z., Atomic coordination environment engineering of bimetallic alloy nanostructures for efficient ammonia electrosynthesis from nitrate. *Proceedings of the National Academy of Sciences* **2023**, e2306461120.

12. Jiacheng Lia; Miao Lia; Ning An; Shuo Zhang; Qinan Song; Yilin Yang; Jing Li; Liu, X., Boosted ammonium production by single cobalt atom catalysts with high Faradic efficiencies. *Proceedings of the National Academy of Sciences* **2022,** *119* (29), e2123450119.

13. Zhao, Y.; Liu, Y.; Zhang, Z.; Mo, Z.; Wang, C.; Gao, S., Flower-like open-structured polycrystalline copper with synergistic multi-crystal plane for efficient electrocatalytic reduction of nitrate to ammonia. *Nano Energy* **2022,** *97*, 107124.

14. Daiyan, R.; Tran-Phu, T.; Kumar, P.; Iputera, K.; Tong, Z.; Leverett, J.; Khan, M. H. A.; Asghar Esmailpour, A.; Jalili, A.; Lim, M.; Tricoli, A.; Liu, R.-S.; Lu, X.; Lovell, E.; Amal, R., Nitrate reduction to ammonium: from CuO defect engineering to waste NO_x-to-NH_3 economic feasibility. *Energy & Environmental Science* **2021,** *14* (6), 3588-3598.

15. Hao, R.; Tian, L.; Wang, C.; Wang, L.; Liu, Y.; Wang, G.; Li, W.; Ozin, G. A., Pollution to solution: A universal electrocatalyst for reduction of all NO_x-based species to NH_3. *Chem Catalysis* **2022,** *2* (3), 622-638.

16. Lu, X.; Yu, J.; Cai, J.; Zhang, Q.; Yang, S.; Gu, L.; Waterhouse, G. I. N.; Zang, S.-Q.; Yang, B.; Lu, S., Exclusive nitrate to ammonia conversion via boron-doped carbon dots induced surface Lewis acid sites. *Cell Reports Physical Science* **2022,** *3* (7), 100961.

17. Wang, Y.; Zhou, W.; Jia, R.; Yu, Y.; Zhang, B., Unveiling the Activity Origin of a Copper‐based Electrocatalyst for Selective Nitrate Reduction to Ammonia. *Angewandte Chemie International Edition* **2020,** *59* (13), 5350-5354.

18. Wang, Y.; Li, H.; Zhou, W.; Zhang, X.; Zhang, B.; Yu, Y., Structurally Disordered RuO_2 Nanosheets with Rich Oxygen Vacancies for Enhanced Nitrate Electroreduction to Ammonia. *Angewandte Chemie International Edition* **2022,** *61* (19), e202202604

19. Lv, F.; Sun, M.; Hu, Y.; Xu, J.; Huang, W.; Han, N.; Huang, B.; Li, Y., Near-unity electrochemical conversion of nitrate to ammonia on crystalline nickel porphyrin-based covalent organic frameworks. *Energy & Environmental Science* **2023,** *16* (1), 201-209.

20. Liu, H.; Lang, X.; Zhu, C.; Timoshenko, J.; Rüscher, M.; Bai, L.; Guijarro, N.; Yin, H.; Peng, Y.; Li, J.; Liu, Z.; Wang, W.; Cuenya, B. R.; Luo, J., Efficient Electrochemical Nitrate Reduction to Ammonia with Copper‐Supported Rhodium Cluster and Single‐Atom Catalysts. *Angewandte Chemie International Edition* **2022,** *61* (23), e202202556.

21. Chen, D.; Zhang, S.; Yin, D.; Li, W.; Bu, X.; Quan, Q.; Lai, Z.; Wang, W.; Meng, Y.; Liu, C.; Yip, S.; Chen, F. R.; Zhi, C.; Ho, J. C., Tailored p‐Orbital Delocalization by Diatomic Pt‐Ce Induced Interlayer Spacing Engineering for Highly‐Efficient Ammonia Electrosynthesis. *Advanced Energy Materials* **2022,** *13* (6), 2203201.

22. Wang, C.; Ye, F.; Shen, J.; Xue, K.-H.; Zhu, Y.; Li, C., In Situ Loading of Cu_2O Active Sites on Island-like Copper for Efficient Electrochemical Reduction of Nitrate to Ammonia. *ACS Applied Materials & Interfaces* **2022,** *14* (5), 6680-6688.

23. Han, Y.; Zhang, X.; Cai, W.; Zhao, H.; Zhang, Y.; Sun, Y.; Hu, Z.; Li, S.; Lai, J.; Wang, L., Facet-controlled palladium nanocrystalline for enhanced nitrate reduction towards ammonia. *Journal of Colloid and Interface Science* **2021,** *600*, 620-628.

24. Wu, Z.-Y.; Karamad, M.; Yong, X.; Huang, Q.; Cullen, D. A.; Zhu, P.; Xia, C.; Xiao, Q.; Shakouri, M.; Chen, F.-Y.; Kim, J. Y.; Xia, Y.; Heck, K.; Hu, Y.; Wong, M. S.; Li, Q.; Gates, I.; Siahrostami, S.; Wang, H., Electrochemical ammonia synthesis via nitrate reduction on Fe single atom catalyst. *Nature Communications* **2021,** *12* (1), 2870.

25. Yin, H.; Chen, Z.; Xiong, S.; Chen, J.; Wang, C.; Wang, R.; Kuwahara, Y.; Luo, J.;

Yamashita, H.; Peng, Y.; Li, J., Alloying effect-induced electron polarization drives nitrate electroreduction to ammonia. *Chem Catalysis* **2021,** *1* (5), 1088-1103.

26. Li, X.; Zhang, G.; Zhang, N.; Luo, Y.; Shen, P.; Li, X.; Chu, K., Regulating Pd nanosheets by W-doping for electrochemical nitrate reduction to ammonia. *New Journal of Chemistry* **2022,** *46* (30), 14724-14730.

27. Li, X.; Zhao, X.; Zhou, Y.; Hu, J.; Zhang, H.; Hu, X.; Hu, G., Pd nanocrystals embedded in BC2N for efficient electrochemical conversion of nitrate to ammonia. *Applied Surface Science* **2022,** *584*, 152556.

28. Song, Z.; Liu, Y.; Zhong, Y.; Guo, Q.; Zeng, J.; Geng, Z., Efficient Electroreduction of Nitrate into Ammonia at Ultralow Concentrations Via an Enrichment Effect. *Advanced Materials* **2022,** *34* (36), 2204306.

29. Liu, Y.; Cheng, R.; Ren, H.; Sun, T.; Liu, D., Ultrasmall Iron Nanoparticle-Decorated Carbon Black for High-Efficiency Nitrate-to-Ammonia Electrosynthesis and Zinc-Nitrate Batteries. *ACS Sustainable Chemistry & Engineering* **2024,** *12* (9), 3780-3789.

30. Ding, J.; Hou, X.; Qiu, Y.; Zhang, S.; Liu, Q.; Luo, J.; Liu, X., Iron-doping strategy promotes electroreduction of nitrate to ammonia on MoS_2 nanosheets. *Inorganic Chemistry Communications* **2023,** *151*, 110621.

31. Wu, S.; Jiang, Y.; Luo, W.; Xu, P.; Huang, L.; Du, Y.; Wang, H.; Zhou, X.; Ge, Y.; Qian, J.; Nie, H.; Yang, Z., Ag‐Co_3O_4‐CoOOH‐Nanowires Tandem Catalyst for Efficient Electrocatalytic Conversion of Nitrate to Ammonia at Low Overpotential via Triple Reactions. *Advanced Science* **2023,** *10* (33), 2303789.

32. Yang, J.; Zhang, W.-D.; Zhao, H.; Zou, Y.; Zhang, Z.-Y.; Liu, J.; Wang, J.; Gu, Z.-G.; Yan, X., High-valent cobalt active sites derived from electrochemical activation of metal-organic frameworks for efficient nitrate reduction to ammonia. *Applied Catalysis B: Environmental* **2024,** *340*, 123237.

33. Zhang, R.; Hong, H.; Liu, X.; Zhang, S.; Li, C.; Cui, H.; Wang, Y.; Liu, J.; Hou, Y.; Li, P.; Huang, Z.; Guo, Y.; Zhi, C., Molecular Engineering of a Metal‐Organic Polymer for Enhanced Electrochemical Nitrate‐to‐Ammonia Conversion and Zinc Nitrate Batteries. *Angewandte Chemie International Edition* **2023,** *62* (48), e202309930.

34. Jiang, H.; Chen, G. F.; Savateev, O.; Xue, J.; Ding, L. X.; Liang, Z.; Antonietti, M.; Wang, H., Enabled Efficient Ammonia Synthesis and Energy Supply in a Zinc–Nitrate Battery System by Separating Nitrate Reduction Process into Two Stages. *Angewandte Chemie International Edition* **2023,** *62* (13), e202218717.

35. Liu, Q.; Xie, L.; Liang, J.; Ren, Y.; Wang, Y.; Zhang, L.; Yue, L.; Li, T.; Luo, Y.; Li, N.; Tang, B.; Liu, Y.; Gao, S.; Alshehri, A. A.; Shakir, I.; Agboola, P. O.; Kong, Q.; Wang, Q.; Ma, D.; Sun, X., Ambient Ammonia Synthesis via Electrochemical Reduction of Nitrate Enabled by $NiCo_2O_4$ Nanowire Array. *Small* **2022,** *18* (13), 2106961.

36. Li, Z.; Liang, J.; Liu, Q.; Xie, L.; Zhang, L.; Ren, Y.; Yue, L.; Li, N.; Tang, B.; Alshehri, A. A.; Hamdy, M. S.; Luo, Y.; Kong, Q.; Sun, X., High-efficiency ammonia electrosynthesis via selective reduction of nitrate on $ZnCo_2O_4$ nanosheet array. *Materials Today Physics* **2022,** *23*, 100619.

37. Li, Z.; Deng, Z.; Ouyang, L.; Fan, X.; Zhang, L.; Sun, S.; Liu, Q.; Alshehri, A. A.; Luo, Y.; Kong, Q.; Sun, X., CeO_2 nanoparticles with oxygen vacancies decorated N-doped carbon nanorods: A highly efficient catalyst for nitrate electroreduction to ammonia. *Nano Research* **2022,** *15*

(10), 8914-8921.

38. Wang, Y.; Hao, F.; Sun, M.; Liu, M. T.; Zhou, J.; Xiong, Y.; Ye, C.; Wang, X.; Liu, F.; Wang, J.; Lu, P.; Ma, Y.; Yin, J.; Chen, H. C.; Zhang, Q.; Gu, L.; Chen, H. M.; Huang, B.; Fan, Z., Crystal Phase Engineering of Ultrathin Alloy Nanostructures for Highly Efficient Electroreduction of Nitrate to Ammonia. *Advanced Materials* **2024,** *36* (14), 2313548.

39. Zhong, W.; Hong, Q. L.; Ai, X.; Zhang, C.; Li, F. M.; Li, X. F.; Chen, Y., RhNi Bimetallenes with Lattice‐Compressed Rh Skin towards Ultrastable Acidic Nitrate Electroreduction. *Advanced Materials* **2024,** *36* (23), 2314351.

40. Chang, Z.; Meng, G.; Chen, Y.; Chen, C.; Han, S.; Wu, P.; Zhu, L.; Tian, H.; Kong, F.; Wang, M.; Cui, X.; Shi, J., Dual‐Site W‐O‐CoP Catalysts for Active and Selective Nitrate Conversion to Ammonia in a Broad Concentration Window. *Advanced Materials* **2023,** *35* (32), 2304508.

41. Jiang, H.; Chen, G. F.; Hai, G.; Wang, W.; Liang, Z.; Ding, L. X.; Yuan, Y.; Lu, J.; Antonietti, M.; Wang, H., A Nitrogen Battery Electrode involving Eight‐Electron Transfer per Nitrogen for Energy Storage. *Angewandte Chemie International Edition* **2023,** *62* (30), e202305695.

42. Wen, W.; Yan, P.; Sun, W.; Zhou, Y.; Yu, X. Y., Metastable Phase Cu with Optimized Local Electronic State for Efficient Electrocatalytic Production of Ammonia from Nitrate. *Advanced Functional Materials* **2022,** *33* (6), 2212236.